



Numerical Assessment of Tsunami Forces on Vertical Wall Structures: Impact of Inundation Depth and Incident Fluid Velocity

Emad Q. Hussein¹, Farhan Lafta Rashid^{1,*}, Najah M. L. Al Maimuri², Ali Basem³, Hayder Ibrahim Mohammed⁴

¹ Petroleum Engineering Department, University of Kerbala, Karbala 56001, Iraq

² Building and Construction Techniques Engineering Department, Al Mustaqbal University, Babylon, Iraq

³ Air Conditioning Engineering Department, Faculty of Engineering, Warith Al-Anbiyaa University, Karbala 56001, Iraq

⁴ Department of Cooling and Air Conditioning Engineering, Imam Ja'afar Al-Sadiq University, Baghdad, Iraq

ARTICLE INFO

Article history:

Received 26 July 2023

Received in revised form 22 August 2023

Accepted 24 September 2023

Available online 3 January 2024

Keywords:

Tsunami Bore Forces; Froude Number; Land Structure; CFD; inundation depth

ABSTRACT

This study evaluates the tsunami forces exerted on a terrestrial structure caused by a collision-induced tsunami. Conventionally, assessing these forces relies on the inundation depth of the colliding tsunami passing without the presence of the terrestrial structure. However, it is essential to consider the inundation depth and incident fluid velocity, as both significantly influence the resulting tsunami forces. In this research, ANSYS Fluent 17.2 is employed to simulate excitation sources using a Defined Function (UDF) code within a C++ framework. The dynamic meshing technique is adopted to replicate the interactions between the bore pressure of the tsunami and an idealised vertical wall structure across three distinct water levels. Computational Fluid Dynamics (CFD) modelling demonstrates the proposed methodology's capability to offer precise impact pressure distributions concerning geographical and temporal aspects. The findings reveal specific instances: at a water depth of 10 m, the maximum Froude number is attained at 3.5 and 6.9 seconds, corresponding to a maximum pressure value of 3.9×10^5 Pa at 3.85 seconds for a water flow velocity of 20 m/sec. Similarly, for a water depth of 12 m, the most significant Froude number is observed at 3.95 and 6.9 seconds, with a peak pressure value of 1.8×10^5 Pa at 4.6 seconds, associated with a water flow velocity of 15 m/s. Additionally, at a water depth of 14 m, the maximum Froude number is reached at 4.95 and 7.1 seconds, accompanied by a maximum pressure value of 7.4×10^4 Pa at 4.85 seconds for a water flow velocity of 10 m/s.

1. Introduction

Numerous nations' coastlines have been devastated by tsunamis in the past. Over the last several years, it has captured the public's attention by demonstrating its resilience in the face of two of history's worst natural disasters: the Great Indian Ocean Tsunami on December 26, 2004, and the 2011 Tohoku Tsunami. Tsunamis are caused by the abrupt movement of a massive volume of water, which mainly produces lengthy gravity waves. Multiple waves are often produced and travel in the

* Corresponding author.

E-mail address: farhan.lefta@uokerbala.edu.iq (Farhan Lafta Rashid)

same direction due to a depression wave or a wave crest. It is quite challenging to forecast the features of a Tsunami since the geography along the coastline varies significantly throughout the sea. This wave often forms offshore and travels inshore as a broken wave. These cylinders may move inland as damaging wave surges after breaching the coast. Several unknown ocean characteristics make it difficult to estimate the pressure of a tsunami on a building, but scientists have nevertheless attempted to measure and forecast wave pressure on various structures via testing and computer modelling [1, 2].

Throughout history, tsunamis have caused severe destruction in several coastal regions across many countries. Notably, on December 26, 2004, one of the worst natural disasters in recorded history occurred, leaving a lasting impression on people's minds for years. The Indian Ocean witnessed this enormous disaster. If coastal infrastructure, which includes buildings, bridges, roads, and harbour facilities, is not designed to resist the powerful force of surging waters, it could suffer severe damage in the event of a tsunami. The harmful effects of the tsunami in the Indian Ocean in 2004 have been investigated in relation to fluid loading and scour damage [3-5]. The structural harm caused by hurricane storm surges and waves can uncannily resemble the harm caused by earthquakes [6, 7]. For instance, flooring damage occurred due to vertical fluid forces during Hurricane Katrina. Although hurricane-related surges, waves, and tsunamis have tremendous destructive force, their fundamental physics are very different [8].

Much study has been done to develop methods for calculating the stresses that wave activities place on buildings. There are three main components to this project. First and foremost, the impact of storm-generated waves on offshore installations has drawn much interest. A wide range of empirical and computational experiments has been conducted to establish load design formulations. The effects of storm waves on coastal defences, such as seawalls and breakwaters, are the second crucial factor. Intriguingly, much research hasn't been done on how tsunami bores and surges affect coastal constructions [9].

Using a model of residential construction, Lindt *et al.*, [10] identified the bore forces connected to tsunamis. Experimental investigations of the effects of tsunami loading on structures with apertures were done by Lukkunaprasit *et al.*, [11]. Numerical analysis was used by Wijatmiko and Murakami [12] to examine the interaction between a tsunami bore and a cylindrical object. Nakamura *et al.*, [13] three-dimensional (3D) computational investigation into the effects of runup and tsunami-induced stresses on the deformation of square buildings furthered the discussion. Through experimental and computational modelling, Nistor *et al.*, [14] investigated the impacts of tsunami loading onto structures. Experimental testing of cylindrical and rectangular vertical systems was part of this project, whereas cylindrical configurations were the subject of numerical investigations. Numerous studies are predicting the actual behavioural patterns in computational fluid dynamics [15-21].

This study's main objective is understanding the complex intricacies underlying fluid pressure interactions when tsunamis approach vertical walls with apertures using a groundbreaking computational fluid dynamics (CFD) application. This study adds something new to the body of knowledge because it explores a topic that hasn't gotten much attention. The main focus of the study is a detailed explanation of the numerical model's complex mechanics and operational structure. The disclosure of findings relating to the dynamic evolution of pressure patterns and the apparent trends in the Froude number parameter is particularly significant. This creative project aims to develop knowledge of how tsunamis interact with structural arrangements that feature apertures, ultimately leading to improvements in our understanding of the resilience of coastal infrastructure.

2. Model Description

The computational geometry model is described in detail in Figure 1. The left side is the entrance surface, the water surface elevation is 10-14 m, the wave height is 0.5 m, and the wavelength is 10 m. The top surface of the model is an open boundary, the same as the atmosphere.

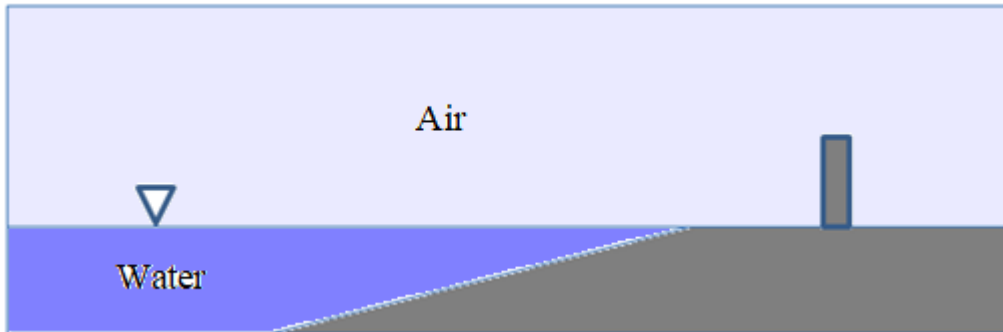


Fig. 1. Schematic diagram of the model description with a simple structure

3. Numerical Model

The 2D transient analysis uses ANSYS Fluent at three different water levels. To demonstrate the behaviour of tsunami bore forces on vertical walls, a multiphase model was created to trace the liquid's free surface using the Volume of Fluid (VOF), and the dynamic meshing technique was used to simulate the excitation sources via the Defined Function (UDF) code in the C++ environment.

The Navies Stokes (NS) equations or Reynolds Averaged Navies Stokes (RANS) equations for 2D or 3D fluid flows may be solved with the help of the computational fluid dynamics (CFD) programme Fluent 17.2. The Fluent base solver used the finite volume method to analyse and exercise discretion over the fluid governing equations solved by RANS with the help of the VOF approach for monitoring the free surface motion. The momentum equation was discretised using a second-order upward technique, and the body-force-weight method used pressure interpolation. To compute the convection and diffusion fluxes via the faces of the control volume, the pressure Implicitly with Operators (PISO) technique is used.

Waves in water are generated using the dynamic mesh approach, except that the function of momentum source was incorporated into the x-momentum equations using the macro of the UDFs in the programme Fluent. The computational results were affected by the grid size and the temporal grid size for a no-slip boundary with smooth boundary conditions.

3.1 Procedure of UDF

The usual features of the fluent programme may be obtained by importing UDF. Initial and boundary conditions and material qualities may be specified for a specific issue. The UDF is written in the C programming language and compiled using visual express compilers. The Fluent software describes several different macros that may be implemented in UDF's code, as is the liquid movement performed by the macro.

3.2 Froude Number (*Fr*)

The Froude number (*Fr*) is a dimensionless quantity defined as the ratio of the inertia of the flow to the external field (often just gravity). To calculate the Froude number, we need the speed-length ratio, which is defined as:

$$Fr = \frac{u}{\sqrt{GH}} \quad (1)$$

Where,

u- is the local flow velocity.

G- is the acceleration of fluid.

H-is the deep of water.

3.3 Mathematical Formulation

A mathematical model and its answers for calculating the bore pressure of a tsunami are presented here. The liquid flow and the free surface motion of water are mathematically modelled. The governing equations were solved using a well-known CFD method, and VOF was employed as the interface capturing strategy because of its sensitivity to phase fraction. The VOF model is used to observe the air-water boundary and, by extension, the wave motion. The continuity equation, the momentum equation, and the phase equation are expressed as the governing equations [22, 23]:

$$\frac{\partial \rho}{\partial t} + \nabla \cdot (\rho u) = 0 \quad (2)$$

$$\rho u / \partial t + \nabla \cdot (\rho u u) - \nabla \cdot \tau = C \kappa \nabla \alpha - gh \nabla \rho - \nabla P_d \quad (3)$$

$$D\alpha / Dt = \partial \alpha / \partial t + \nabla \cdot (\alpha u) = 0 \quad (4)$$

This work sets the surface tension coefficient, *C*, to zero. Also, the gravity acceleration, *g*, the volume fraction, *α*, the position vector *h*, and the dynamic pressure, *P_d*, are defined as follows: where *ρ* is the density, *u* is the velocity vector of the fluid, *K* is the curvature of the interface, and *C* is the velocity of sound through the liquid. Stress due to shear (*τ*). The shear stress is measured to monitor the free surface and phase interface. The density may be calculated using the following formula, where *ρ₁*, *ρ₂* are the densities of air and water, respectively [24-33].

$$\rho = \alpha \rho_1 + (1 - \alpha) \times \rho_2 \quad (5)$$

The dynamic viscosities of the two fluids are (*μ₁*, *μ₂*), which can be determined by the following equation:

$$\mu = \alpha \mu_1 + (1 - \alpha) \times \mu_2 \quad (6)$$

The coefficient of the phase function (*α*) may be considered the liquid density in the domain per unit volume. This indicates that the cell is full of liquid if it is unity. And if *α* = 0, the compartment is filled with air.

4. Results and Discussion

In this study, ANSYS Fluent 17.2 is used as a key tool to carefully record and model the complex interactions that arise between a tsunami's bore pressure and a hypothetical vertical wall structure. This research spans a variety of scenarios with three different water levels, enabling a thorough comprehension of the complex dynamics underlying these interactions.

As shown in Figures 2 and 3, a thorough visualization of density and pressure contours is shown before the water and vertical wall collide. The wave height is 0.5 m, the typical wavelength is 10 m, the water flow velocity is 20 m/sec, and the significant water depth is 10 m. The delicate distribution of density and pressure as the water approaches the vertical wall may be seen in these graphic representations, which also provide an overview of the subtle hydrodynamic forces at work.

On the other hand, Figures 4 and 5 provide insight into how the density and pressure contours changed during the crucial contact between the water and the vertical wall. These illustrations provide a visual account of the significant alterations that the fluid medium experiences when it encounters the structural barrier. The displayed pressure and density changes offer a concrete representation of the fluid's transient reaction and the resulting pressure distribution, illuminating the subtleties of fluid-structure interaction in this situation.

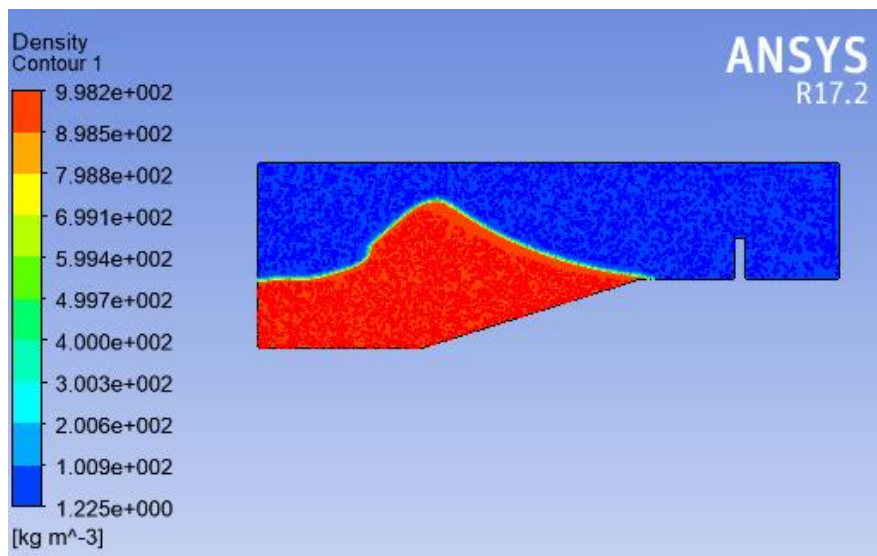


Fig. 2. Density contour before the collision of water with vertical wall

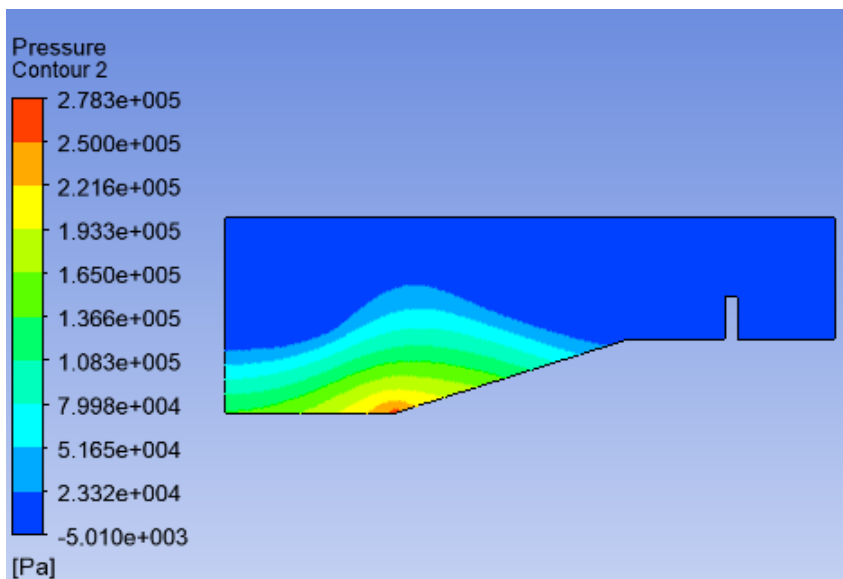


Fig. 3. Pressure contour before collision of water with vertical wall

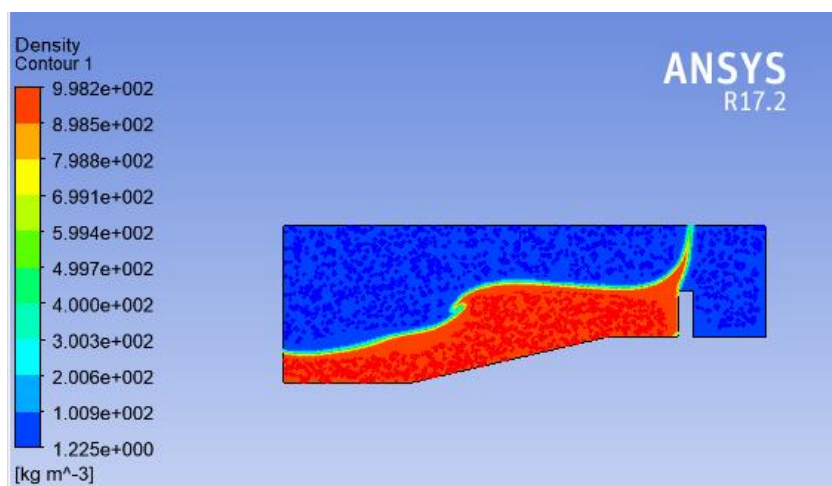


Fig. 4. Density contour during the collision of water with vertical wall

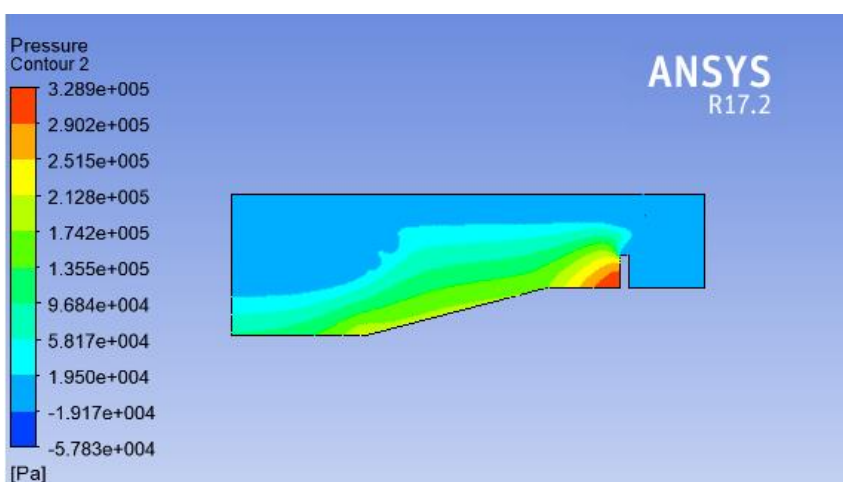


Fig. 5. Pressure contour during the collision of water with vertical wall

The outcomes of four cases are provided in Table 1. The cases are designated 1, 2, 3, and 4.

Table 1

The offered scenarios are for various flow velocities and water depths

Case no.	Wave height (m)	Depth of water (m)	Wavelength (m)	Flow velocity (m/s)
1	0.5	10, 12, 14	10	20
2	0.5	10, 12, 14	10	15
3	0.5	10, 12, 14	10	10
4	0.5	10	10	10, 15, 20

Figure 6 shows time histories of the resulting Froude numbers at different water depths (10, 12, and 14 m) with a water flow velocity of 20 m/sec. The median, lowest, and maximum values for every water depth are shown in the inset of Figure 6. The water depth of 14 m has greater values in Froude numbers than the other depth till 3.3 seconds and then is less than the other after this point. The maximum Froude number can be obtained at 3.5 and 6.9 seconds for a water depth of 10 m.

Time histories of the total pressure on the wall specimen at three distinct water depths (10, 12, and 14 m) and one water flow velocity (20 m/sec) are shown in Figure 7. The timeline begins just before the first wall load measurement. Take note of the several vertical scales used to clarify the graphic. As it travels through the flat reef, the bore's leading-edge turbulence contributes to the temporal differences between otherwise similar incoming waves. The maximum pressure value was 3.9×10^5 Pa, which occurred for a water depth of 10 m at 3.85 seconds.

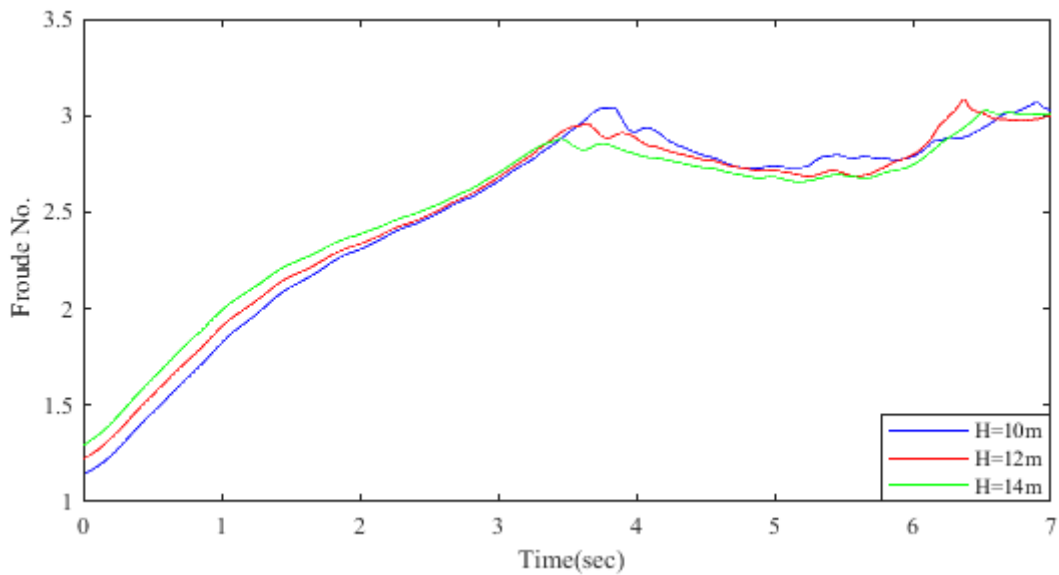


Fig. 6. Froude no. variation at different water depths with a flow velocity of 20 m/sec

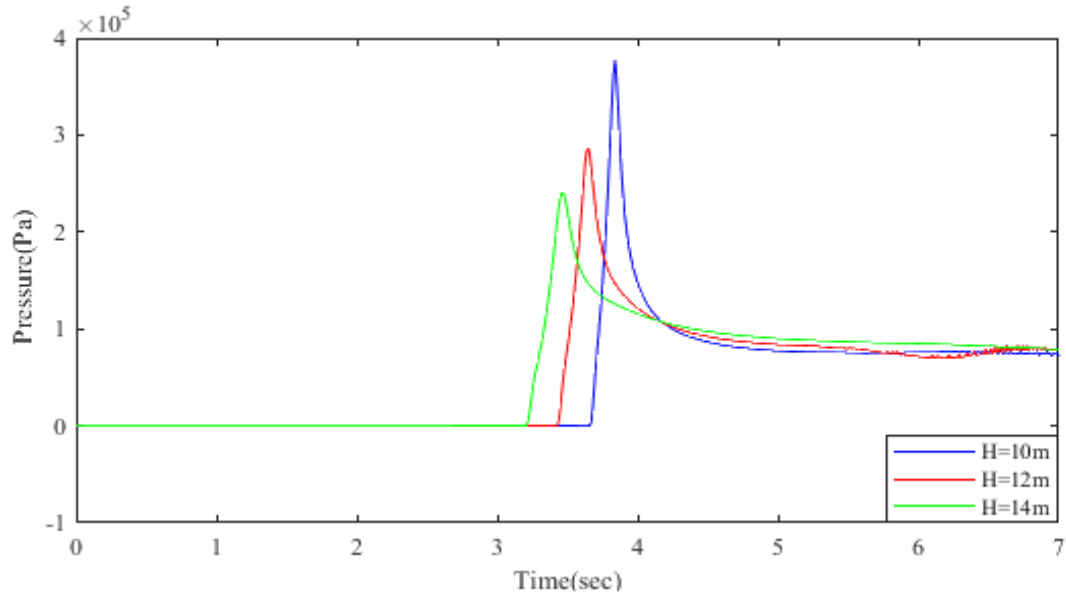


Fig. 7. Pressure variation on the vertical wall at different water depths with a flow velocity of 20 m/sec

Figure 8 shows time histories of the resulting Froude numbers at different water depths (10, 12, and 14 m) with water flow velocity of 15 m/sec. The median, lowest, and maximum values for every water depth are shown in the inset of Figure 8. The water depth of 14 m has greater values in Froude numbers than the other depth till 3.95 seconds, then fluctuated after this time. The maximum Froude number can be obtained at 3.95 and 6.9 seconds for a water depth of 14 m.

Time histories of the total pressure on the wall specimen are shown in Figure 9 for three different water depths (10, 12, and 14 m) and a water flow velocity of 15 m/sec. The timeline begins just before the first wall load measurement. Take note of the several vertical scales used to clarify the graphic. As it travels through the flat reef, the bore's leading-edge turbulence contributes to the temporal differences between otherwise similar incoming waves. The maximum pressure value was 1.8×10^5 Pa, which occurred for a water depth of 10 m at 4.6 seconds.

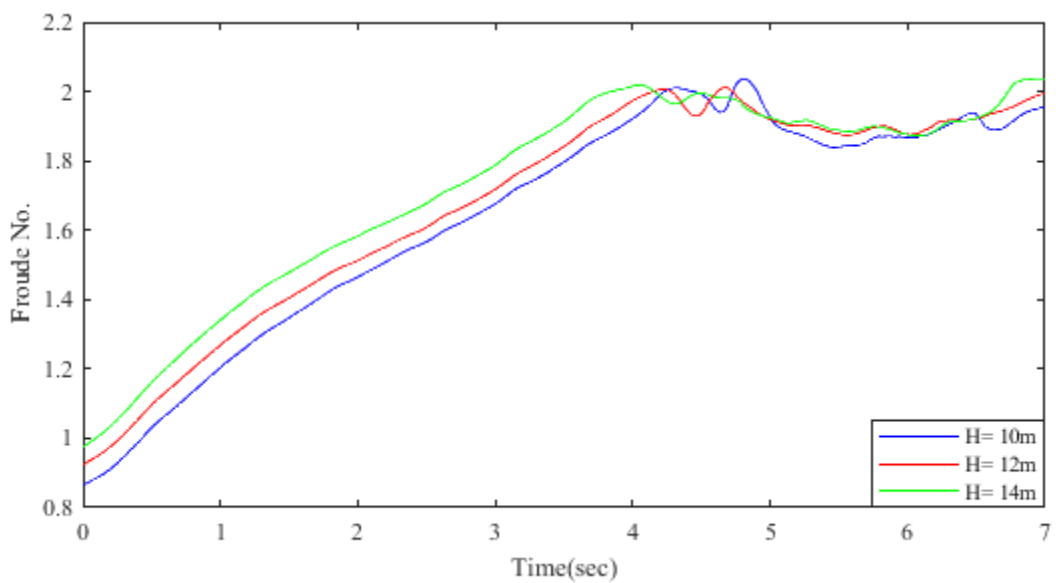


Fig. 8. Froude no. variation at different water depths with a flow velocity of 15 m/sec

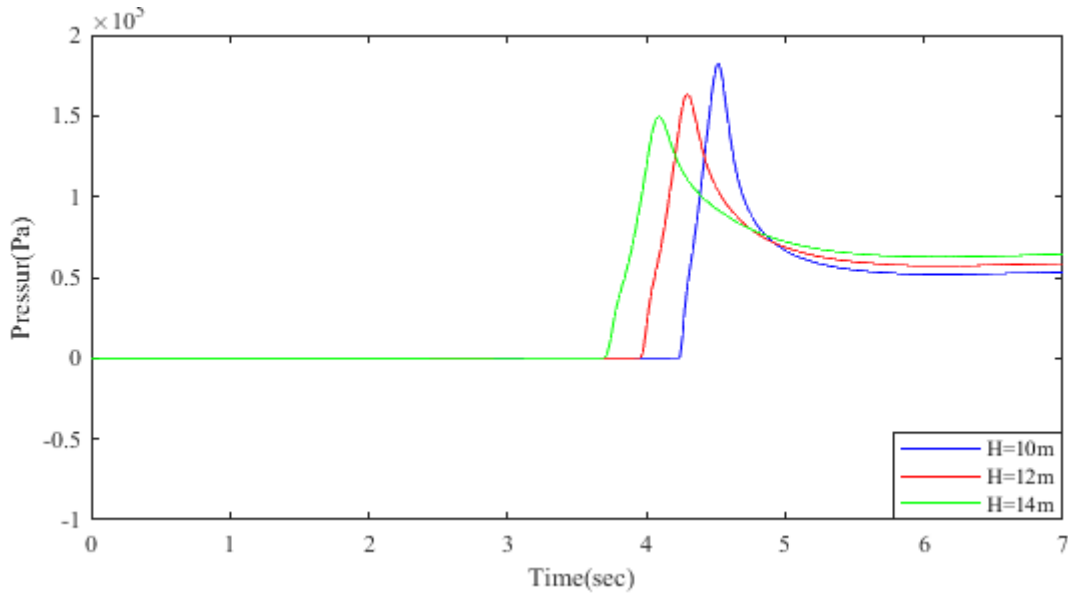


Fig. 9. Pressure variation in the obstruct at different water depths with a flow velocity of 15 m/sec

Figure 10 shows time histories of the resulting Froude numbers at different water depths (10, 12, and 14 m) with a water flow velocity of 10 m/sec. Figure 10 has an inset showing average, minimum, and maximum values for all water depths. The water depth of 14 m always has greater values in Froude numbers than the other depths. The maximum Froude number can be obtained at 4.95 and 7.1 seconds for a water depth of 14 m.

Time histories of the total pressure on the wall specimen at depths of 10, 12, and 14m and a water flow rate of 10m per second are shown in Figure 11. The timeline begins just before the first wall load measurement. Take note of the several vertical scales used to clarify the graphic. As it travels through the flat reef, the bore's leading-edge turbulence contributes to the temporal differences between otherwise similar incoming waves. The maximum pressure value was 7.4×10^4 Pa, which occurred for a water depth of 14 m at 4.85 seconds.

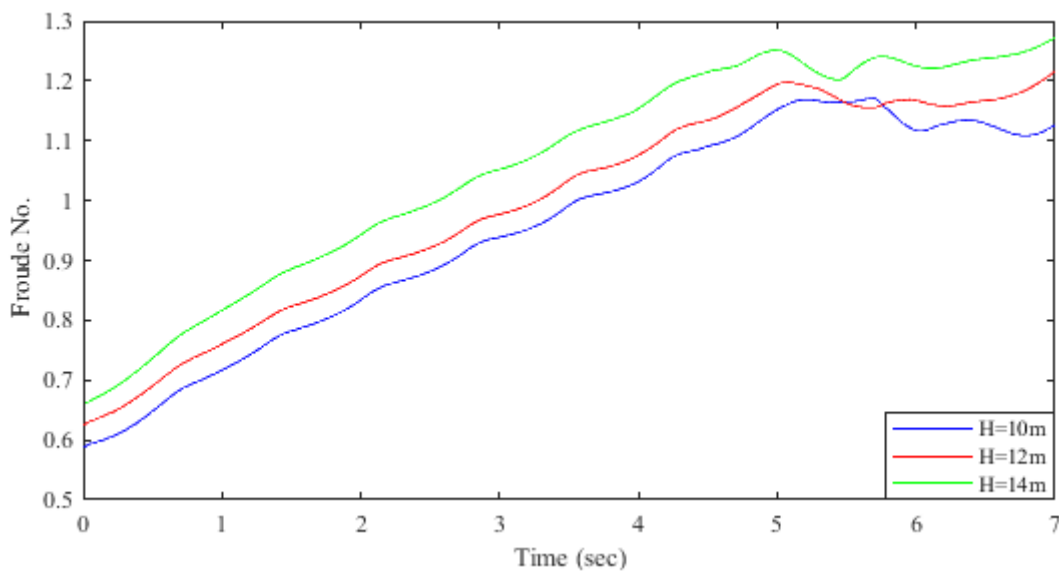


Fig. 10. Froude no. variation at different water depths with a flow velocity of 10 m/sec

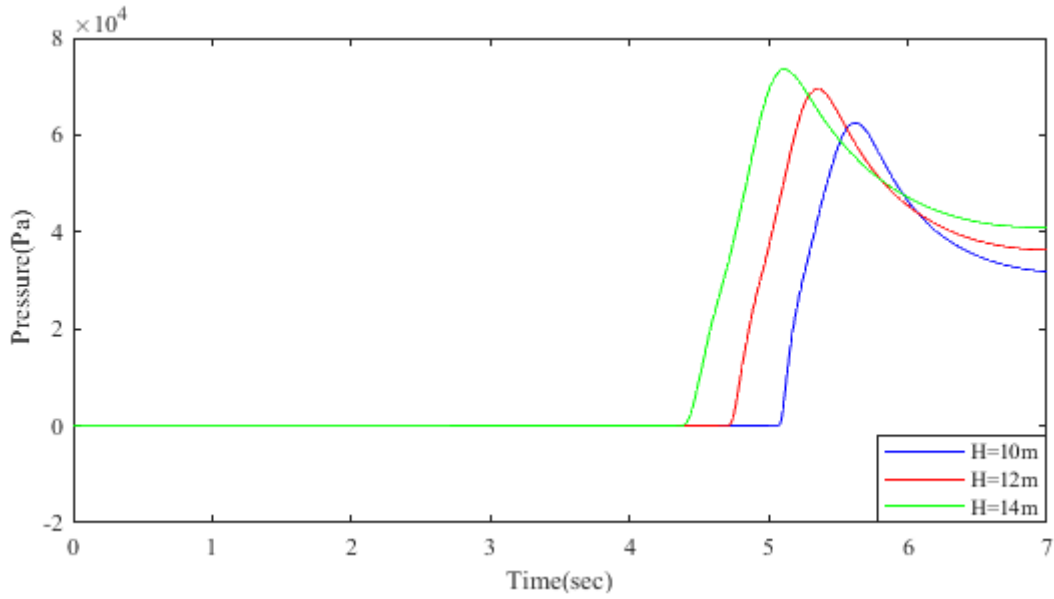


Fig. 11. Pressure variation in the obstruct at different water depths with a flow velocity of 10 m/sec

Figure 12 shows time histories of Froude number for a water depth of 10 m with different flow velocities. The median, minimum, and maximum values for every water depth are shown in the inset of Figure 12. The flow velocity of 20 m/s always has greater values in Froude numbers than the other depths. The maximum Froude number can be obtained at 3.5 and 6.9 seconds.

For a water depth of 10m and varying flow velocities, the time histories of the total pressure on the wall specimen are shown in Figure 13. The timeline begins just before the first wall load measurement. Take note of the several vertical scales used to clarify the graphic. As it travels through the flat reef, the bore's leading-edge turbulence contributes to the temporal differences between otherwise similar incoming waves. The maximum pressure value was 3.9×10^5 Pa, which occurred for a water flow velocity of 20 m/s at 3.85 seconds.

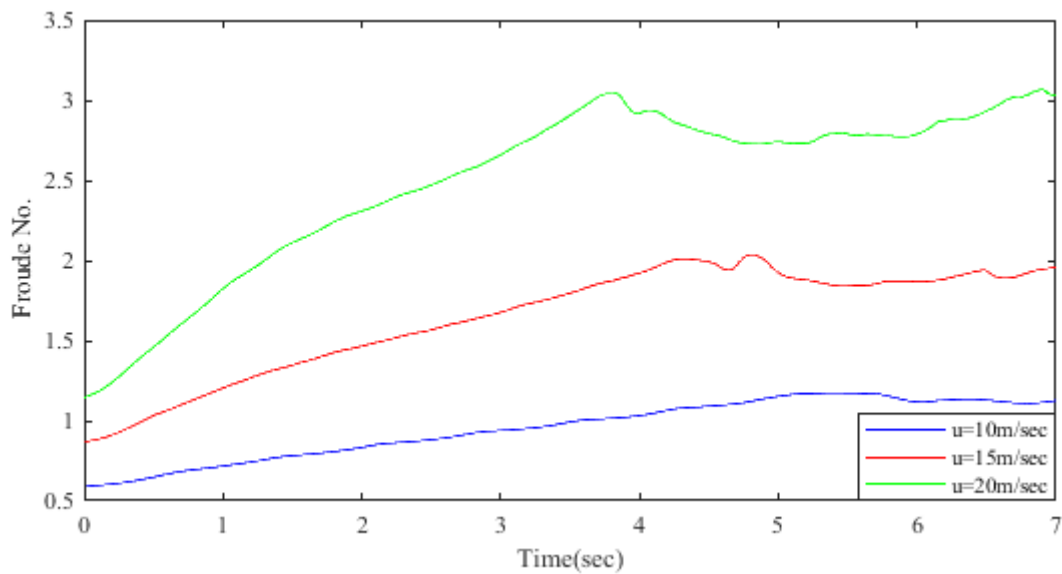


Fig. 12. Froude no. variation at the deep of water 10 m with different velocity

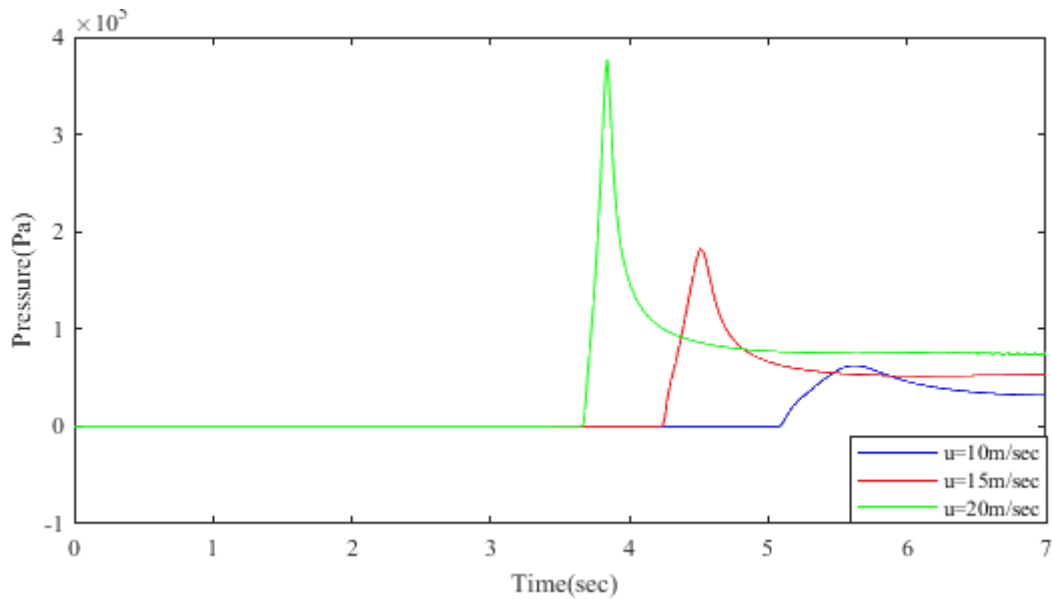


Fig. 13. Pressure variation in the obstruct at the deep of water 10 m with different flow velocities

5. Conclusion

This study uses an exclusively Defined Function (UDF) code within a C++ framework to harness ANSYS Fluent 17.2 to conduct simulations utilising excitation sources. Using the dynamic meshing technique, we carefully simulate interactions between the bore pressure caused by a tsunami and an idealised vertical wall structure over three different water levels. The study skilfully demonstrates the method's prowess in delivering impact pressure distributions that are spatially precise and temporally accurate through meticulous Computational Fluid Dynamics (CFD) simulations. The findings of our analysis, which highlight essential tendencies, serve as its primary focus. The results show a striking pattern: when high flow velocity values are present, the largest Froude numbers appear at shallower water depths. It's interesting to note that the analysis also reveals a distinctive feature about pressure dynamics. Contrary to Froude numbers, the maximum pressure levels are seen in situations with higher water velocities and depths. Underscoring the intricate complexity of tsunami-structure interactions, this fascinating interplay of Froude numbers and pressure magnitudes across various ocean conditions offers crucial insights for comprehending and building resilient coastal structures.

References

- [1] CE, S. (1986). *The runup of long waves*. PhD thesis. Caltech, California.
- [2] Ghosh, D., A. K. Mittal, and S. K. Bhattacharyya. "Multiphase modeling of tsunami impact on building with openings." *The Journal of Computational Multiphase Flows* 8, no. 2 (2016): 85-94. <https://doi.org/10.1177/0010836716653881.cmf.sagepub.com>
- [3] Hiroi, I. "A formula for evaluating breaking wave pressure intensity in the case of breaking waves." *Journal of the College of Engineering, Tokyo Imperial University, Tokyo, Japan* (1919): 11-21.
- [4] Yeh, Harry, Mathew Francis, Curt Peterson, Toshitaka Katada, G. Latha, R. K. Chadha, J. P. Singh, and G. Raghuraman. "Effects of the 2004 great Sumatra tsunami: Southeast Indian coast." *Journal of waterway, port, coastal, and ocean engineering* 133, no. 6 (2007): 382-400.
- [5] Sundar, V., S. A. Sannasiraj, K. Murali, and R. Sundaravadivelu. "Runup and inundation along the Indian peninsula, including the Andaman Islands, due to Great Indian Ocean Tsunami." *Journal of waterway, port, coastal, and ocean engineering* 133, no. 6 (2007): 401-413.

- [6] Robertson, Ian N., H. Ronald Riggs, Solomon Yim, and Yin Lin Young. "Lessons from Katrina." *Civil Engineering Magazine Archive* 76, no. 4 (2006): 56-63.
- [7] Robertson, Ian N., H. Ronald Riggs, Solomon C. Yim, and Yin Lu Young. "Lessons from Hurricane Katrina storm surge on bridges and buildings." *Journal of Waterway, Port, Coastal, and Ocean Engineering* 133, no. 6 (2007): 463-483.
- [8] Robertson, I. N., H. R. Riggs, and A. Mohamed. "Experimental results of tsunami bore forces on structures." In *International Conference on Offshore Mechanics and Arctic Engineering*, vol. 48180, pp. 509-517. 2008.
- [9] Robertson, I. N., K. Paczkowski, H. R. Riggs, and A. Mohamed. "Tsunami bore forces on walls." In *International Conference on Offshore Mechanics and Arctic Engineering*, vol. 44335, pp. 395-403. 2011.
- [10] van de Lindt, John W., Rakesh Gupta, Rachel A. Garcia, and Jebediah Wilson. "Tsunami bore forces on a compliant residential building model." *Engineering Structures* 31, no. 11 (2009): 2534-2539. <https://doi.org/10.1016/j.engstruct.2009.05.017>
- [11] Lukkunaprasit, P., A. Ruangrassamee, and N. Thanasisathit. "Tsunami loading on buildings with openings." *Science of Tsunami Hazards* 28, no. 5 (2009): 303.
- [12] Wijatmiko, I., and K. Murakami. "Numerical simulation of tsunami bore pressure on cylindrical structure." *Annual Journal of Civil Engineering in the Ocean, JSCE* 26 (2010): 273-278.
- [13] Nakamura, Tomoaki, Norimi Mizutani, and Koji Fujima. "Three-dimensional numerical analysis on deformation of run-up tsunami and tsunami force acting on square structures." In *Proc. 32nd Int. Conf. on Coastal Eng*, vol. 32, pp. 14-10. ASCE, 2010.
- [14] Nistor, Ioan, Dan Palermo, Andrew Cornett, and Taofiq Al-Faesly. "Experimental and numerical modeling of tsunami loading on structures." *Coastal Engineering Proceedings* 32 (2011): 2-2.
- [15] Elhadad, Alaaeldeen M., and Abo El-Ela. "Experimental and CFD Resistance Validation of Naval Combatant Dtm 5415 Model." *Experimental and Cfd Resistance Validation of Naval Combatant Dtm 5415*.
- [16] Kit, Lam Wai, Hassan Mohamed, Ng Yee Luon, and Leon Chan. "Numerical Simulation of Ventilation in a Confined Space." *Journal of Advanced Research in Fluid Mechanics and Thermal Sciences* 107, no. 1 (2023): 1-18. <https://doi.org/10.37934/arfmts.107.1.118>
- [17] Soundrapaman, Allison, Normayati Binti Nordin, Abdoulhdi A. Borhana Omran, and Abdulhafid MA Elfaghi. "Numerical Investigation of Heat Transfer Enhancement of Al₂O₃ Nanofluid in Microchannel Heat Sink." *Journal of Advanced Research in Fluid Mechanics and Thermal Sciences* 107, no. 1 (2023): 19-28. <https://doi.org/10.37934/arfmts.107.1.1928>
- [18] Bachok, Norfifah, Siti Nur Nazurah Tajuddin, Nur Syazana Anuar, and Haliza Rosali. "Numerical Computation of Stagnation Point Flow and Heat Transfer over a Nonlinear Stretching/Shrinking Sheet in Hybrid Nanofluid with Suction/Injection Effects." *Journal of Advanced Research in Fluid Mechanics and Thermal Sciences* 107, no. 1 (2023): 80-86. <https://doi.org/10.37934/arfmts.107.1.8086>
- [19] Babaei-Mahani, Roohollah, Pouyan Talebizadeh Sardari, Salman Masoudi Soltani, Hayder I. Mohammed, Zbigniew Kuncewicz, and Christine Starr. "CFD simulation of a shell and multiple tubes condensing heat exchanger in a modified microwave plant applied for reprocessing End of Life Tires (ELTs)." *Environmental Quality Management* (2023). <https://doi.org/10.1002/tqem.21971>
- [20] Mohammed, Hayder I., Donald Giddings, Gavin S. Walker, and Henry Power. "CFD assessment of the effect of nanoparticles on the heat transfer properties of acetone/ZnBr₂ solution." *Applied Thermal Engineering* 128 (2018): 264-273. <https://doi.org/10.1016/j.applthermaleng.2017.08.169>
- [21] Mohammed, Hayder I. "Discharge improvement of a phase change material-air-based thermal energy storage unit for space heating applications using metal foams in the air sides." *Heat Transfer* 51, no. 5 (2022): 3830-3852. <https://doi.org/10.1002/htj.22479>
- [22] Godderidge, Bernhard, Stephen Turnock, Mingyi Tan, and Chris Earl. "An investigation of multiphase CFD modelling of a lateral sloshing tank." *Computers & Fluids* 38, no. 2 (2009): 183-193. <https://doi.org/10.1016/j.compfluid.2007.11.007>
- [23] Suyal, Rohit. "CFD Analysis of Fuel Sloshing in a Cylindrical Tank with and Without Baffles Under Linear Acceleration." PhD diss., 2016.
- [24] Gatte, Mohammed Taih, Rasim Azeez Kadhim, and Farhan Leftah Rasheed. "Using water energy for electrical energy conservation by building of micro hydroelectric generators on the water pipelines that depend on the difference in elevation." In *2010 1st International Conference on Energy, Power and Control (EPC-IQ)*, pp. 379-383. IEEE, 2010.
- [25] Al Maimuri, Najah ML, A. A. R. Al Tahir, Farhan Lafta Rashid, and Arkan Radi Ali. "Electro-Hydrodynamic Design of an Intelligent Balloon Water Gate Controlled by an Efficient Maximum-Power-Seeking Controller for a Solar Generation System." *IEEE Access* 7 (2019): 157766-157782.
- [26] Hussein, Emad Qasem, Basim Raheem, and Farhan Lafta. "Fluid Structure Interaction of Non-Return Valve Using CFD." *Journal of Mechanical Engineering Research and Developments* 43, no. 7 (2020): 137-148.

- [27] Al-Zughaibi, A. I., E. Q. Hussein, and F. L. Rashid. "A dynamic meshing technique for analysis of nonlinear sloshing in liquid tanks." In *IOP Conference Series: Materials Science and Engineering*, vol. 1067, no. 1, p. 012094. IOP Publishing, 2021. <https://doi.org/10.1088/1757-899X/1067/1/012094>
- [28] Al-Zughaibi, Ali I., Emad Q. Hussein, and Farhan Lafta Rashid. "Studying and analysis of nonlinear sloshing (vibrating) of interaction fluid structure in storage tanks." *J. Mech. Eng. Res. Dev* 7 (2021): 180-191.
- [29] Rashid, Farhan Lafta, Emad Qasem Hussein, Mudhar A. Al-Obaidi, and Awesar A. Hussain. "Numerical Simulation of a Partly Filled Rectangular Tank with Fuel Oil." *Journal of Techniques* 5, no. 3 (2023): 42-51. <https://doi.org/10.51173/jt.v5i3.1465>
- [30] Ali, A.R., Al-Sa'adi, A.M., Hussein, A.A., Al Maimuri, N.M., Hussein, E.Q., Rashid, F.L., Al Mamouri, Z.N., and Albadry, A.M. "Reversible Pendulum Motion of Flexible Walls to Absorb Tsunami Wave's Momentum: A Step for Urban and Regional Planning at Risk." *AIP Conference Proceedings* 2775, 060008 (2023). <https://doi.org/10.1063/5.0141030>.
- [31] Hussain, Awesar A., Mudhar A. Al-Obaidi, and Farhan Lafta Rashid. "Modeling of drag coefficient under emergent and submerged flexible vegetated flow." *Physics of Fluids* 35, no. 6 (2023).
- [32] Ahmad, Shabbir, Kashif Ali, Tanveer Sajid, Umaima Bashir, Farhan Lafta Rashid, Ravinder Kumar, Mohamed R. Ali, Ahmed S. Hendy, and Adil Darvesh. "A novel vortex dynamics for micropolar fluid flow in a lid-driven cavity with magnetic field localization—A computational approach." *Ain Shams Engineering Journal* (2023): 102448. <https://doi.org/10.1016/j.asej.2023.102448>.
- [33] Ahmad, Shabbir, Kashif Ali, Assad Ayub, Umaima Bashir, Farhan Lafta Rashid, Yashar Aryanfar, Mohamed R. Ali, Ahmed S. Hendy, Ismail Shah, and Liaqat Ali. "Localized magnetic fields and their effects on heat transfer enhancement and vortices generation in tri-hybrid nanofluids: A novel investigation." *Case Studies in Thermal Engineering* 50 (2023): 103408. <https://doi.org/10.1016/j.csite.2023.103408>.